Investigation of grain boundaries in $BaSi_2$ epitaxial films on Si(111) substrates using transmission electron microscopy and electron-beam-induced current technique

Masakazu Baba[a], Katsuaki Toh[a], Kaoru Toko[a], Noriyuki Saito[b], Noriko Yoshizawa[b], Karolin Jiptner[c], Takashi Sekiguchi[c], Kosuke Hara[d], Noritaka Usami[d,e] and Takashi Suemasu[a,e]

[a]*Institute of Applied Physics, University of Tsukuba, 1-1-1 Tennohdai, Tsukuba, Ibaraki 305-8573, Japan*

[b]*Electron Microscope Facility, IBEC Innovation Platform, AIST, 16-1 Onogawa, Tsukuba 305-8569, Japan*

[c]*Advanced Electronic Materials Center, National Institute for Materials Science, Tsukuba, Ibaraki 305-0044, Japan*

[d]*Institute for Materials Research, Tohoku University, Sendai 980-8577, Japan*

[e]*Japan Science and Technology Agency, CREST, Chiyoda-ku, Tokyo 102-0075, Japan*

Keywords: A3. Molecular beam epitaxy; B2. Semiconductor silicon compounds

21

22 *a*-Axis-oriented undoped *n*-$BaSi_2$ epitaxial films were grown on Si(111) substrates by
23 molecular beam epitaxy, and the crystalline quality and grain boundaries were investigated by
24 means of reflection high-energy electron diffraction, X-ray diffraction, and transmission
25 electron microscopy (TEM). The grain size of the $BaSi_2$ films was estimated to be
26 approximately 0.1-0.3 μm, and straight grain boundaries (GBs) were observed in the
27 plan-view TEM images. Dark-field TEM images under two-beam diffraction conditions
28 showed that these GBs consist mostly of $BaSi_2$ {011} planes. The diffusion length of minority
29 carriers in *n*-$BaSi_2$ was found to be approximately 10 μm by an electron-beam-induced
30 current technique.

31

32 **1. Introduction**

33 Solar cells have recently been receiving considerable interest as a next-generation
34 energy source to replace conventional sources such as oil and coal. Approximately 90% of
35 solar cells are made from silicon owing to its abundance in the earth's crust, its well-known
36 semiconducting properties and established handling technologies. The production of Si solar
37 cells has been increasing year over year, and this trend is anticipated to continue in the future.
38 However, it is difficult to realize high-efficiency thin-film solar cells using crystalline Si
39 because the absorption coefficient is as small as approximately 10^3 cm^{-1} at 1.5 eV and the
40 band gap is 1.1 eV. These properties are not suitable for high-efficiency thin-film solar cells
41 [1]. Therefore, other novel Si-based materials are of great interest for solar cells. We have
42 specifically targeted realizing *pn* junction solar cells using semiconducting barium disilicide
43 ($BaSi_2$). Composed of the abundant Ba and Si, $BaSi_2$ has a very large absorption coefficient of
44 3×10^4 cm^{-1} at 1.5 eV, and a band gap of 1.3 eV, matching the solar spectrum [2-4]. Thus,
45 $BaSi_2$ is considered to be an alternative new material to Si. Recent achievements of large
46 photoresponsivity of $BaSi_2$ epitaxial layers formed on Si(111) substrates and polycrystalline
47 $BaSi_2$ layers on SiO_2 substrates have spurred interest in this material [5-7]. Orthorhombic
48 $BaSi_2$ is stable under ambient conditions and room temperature (RT), with lattice constants of
49 a=0.891, b=0.672, and c=1.153 nm [8-10]. This material can be grown epitaxially on a
50 Si(111) substrate with the orientation alignment of $BaSi_2$(100)//Si(111), with a small lattice

51 mismatch of 1.0% for $BaSi_2$[010]//Si[112] and 0.1% for $BaSi_2$[001]//Si[110] [11]. The grain

52 size of $BaSi_2$ can be as small as approximately 0.1 μm [12], due to three epitaxial variants

53 rotating around each other by 120° with respect to the surface normal [13,14]. Many grain

54 boundaries (GBs) and other defects in a film typically deteriorate optical and electrical

55 properties of the film. Thus, it is very important to investigate the GBs character in $BaSi_2$. In

56 the case of polycrystalline Si, GBs enhance carrier recombination due to their high defect

57 densities [15], however this recombination activity depends significantly on the GB character

58 due to the difference in the ability of gettering impurities. For example, low-Σ GBs such as Σ3

59 do not act as defect centers of minority carriers [16]. On the other hand, it is thought that

60 recombination of carriers is suppressed by the local built-in potential at the GBs in the case of

61 GBs in $Cu(InGa)Se_2$ [17]. However, there have been no reports thus far on GBs in $BaSi_2$

62 epitaxial films. The diffusion length of minority carriers, a key parameter determining the

63 performance of solar cells, has yet to be evaluated in $BaSi_2$. The electron-beam-induced

64 current (EBIC) technique is considered to be a powerful method for investigating the

65 electrical properties of various semiconductor materials [18].

66 In this study, we grew *a*-axis-oriented $BaSi_2$ epitaxial films on Si(111) substrates by

67 molecular beam epitaxy (MBE) and examined the GBs by transmission electron microscopy

68 (TEM). It was found, from plan-view TEM images and selected-area electron diffraction

69 (SAED) patterns, that the GBs in these $BaSi_2$ epitaxial films are composed mostly of

70 $BaSi_2$ {011} planes. We also evaluated the minority-carrier (holes) diffusion length in *n*-type

71 $BaSi_2$ epitaxial layers using the EBIC technique.

72

73 **2. Experimental procedures**

74 A two-stage growth method was adopted, which included reactive deposition epitaxy

75 (RDE; Ba deposition on hot Si) and molecular beam epitaxy (MBE; co-deposition of Ba and

76 Si) to form thick $BaSi_2$ films [10]. The RDE process was carried out for deposition of a

77 template layer as a $BaSi_2$ precursor prior to the subsequent MBE process [13,14]. The same

78 growth method was successfully utilized for the epitaxial growth of semiconducting β-$FeSi_2$

79 films on both Si(001) and Si(111) substrates [19,20]. An ultrahigh vacuum (UHV) chamber

80 equipped with a Knudsen cell for Ba and an electron beam gun for Si was employed. Before

81 the growth, the *n*-Si substrates (ρ= 0.1 Ω·cm) were prepared by subjecting them to the

82 following treatment. The substrates were washed using RCA clean steps, which removed

83 organic and metallic contaminants. The substrates were then annealed at 830 °C for 30 min in

84 the UHV (1×10^{-6} Pa) chamber to remove the protective SiO_2 layers. After annealing, a 7×7

85 streaky reflection high-energy electron diffraction (RHEED) pattern was observed, indicating

86 a clean Si surface.

87 We fabricated 300-nm-thick undoped *n*-$BaSi_2$ films by RDE at 550 °C for 5 min,

88 followed by MBE at 600 °C for 120 min. Undoped $BaSi_2$ shows *n*-type conductivity with

89 electron concentrations of approximately 10^{16} cm^{-3} [2]. The crystalline quality of the films

90 was evaluated using RHEED and θ-2θ X-ray diffraction (XRD) measurements. In order to

91 investigate the grain size of $BaSi_2$ and GBs, plan-view TEM samples prepared by mechanical

92 polishing and ion milling were observed using TOPCON EM-002B operated at 120 kV. For

93 EBIC measurements, Al/*n*-$BaSi_2$ Schottky diode was formed. Front-side Schottky contacts

94 were formed with Al on the $BaSi_2$ surface via wire bonding, and the back-side ohmic contact

95 was made with Al by sputtering. EBIC observations were carried out in the edge-scan

96 configuration with a Hitachi S4300 field-emission scanning electron microscope (SEM) in the

97 EBIC mode at RT [16]. The acceleration voltage of the electron beam, V_{ac}, was set at 5 kV to

98 avoid penetration of the beam into the Si substrate. The penetration depth of the electron

99 beam is estimated to be shorter than 300 nm, which is the thickness of the $BaSi_2$ layers, when

100 V_{ac} is 5 kV, with the density of $BaSi_2$ being 5.14 g/cm^3.

101

102 **3. Results and discussion**

103 Figure 1(a) shows RHEED patterns of MBE-grown $BaSi_2$ observed along the Si

104 [1-10] azimuth. Sharp streaky patterns of $BaSi_2$ can be seen. Figure 1(b) shows the θ-2θ XRD

105 patterns from the sample. Diffraction peaks can be seen only from (100)-oriented $BaSi_2$

106 planes, such as the (200), (400) and (600) planes. These results indicate that highly

107 *a*-axis-oriented $BaSi_2$ epitaxial films were grown.

108 Figure 2(a) shows a bright-field (BF) plan-view TEM image of the $BaSi_2$. The

109 incident electron beam direction was almost parallel to the $BaSi_2$ [100] zone axis, but was

110 slightly tilted for the GBs to be seen clearly. Because GBs are parallel to the surface normal,

111 their contrast vanishes in the exact [100] zone axis. The $BaSi_2$ grain size is approximately

112 0.1-0.3 μm. We should also note here that approximately 120° sharp GBs are present, and

113 these GBs tend to align along specific directions. Figure 2(b) presents the SAED pattern

114 obtained from the area including several $BaSi_2$ grains in the [100] zone axis. Considering that

115 the GBs are caused by three different *a*-axis-oriented $BaSi_2$ epitaxial variants rotated from

116 each other by 120° with respect to the surface normal [14], the (002), (011), and (020) spots

117 can be grouped into three, shown in red, green, and blue colors in Fig. 2(b). Considering the

118 green and blue epitaxial variants, for example, the green (011) plane is parallel to the blue

119 (002) plane. Thus, it can be stated that the grain boundary indicated by the white dotted line in

120 Fig. 2(a) is composed of the green (011) plane and/or blue (002) plane. It is difficult to

121 distinguish the green (011) plane from the blue (002) plane in the SAED pattern because their

122 lattice spacing, d, is almost the same, that is, $d_{(011)}$=0.586 nm, and $d_{(002)}$=0.579 nm,

123 respectively.

124 Figure 3(a) shows SAED patterns obtained from single grain regions under

125 two-beam diffraction conditions. The diffraction vectors **g** were set to be <004> for the three

126 epitaxial variants shown by blue, red and green in Fig. 2(b). Under these conditions, the

127 diffraction spot corresponding to the (004) plane becomes bright, as seen in Fig. 3(b), while
128 other spots denoted by (00n) (n=±1,±2,±3,...) can also be seen. These facts can help to
129 distinguish (002) plane from (011) plane.

130 Figures 4(a)-4(c) show dark-field (DF) plan-view TEM images using <004> plane
131 reflections observed at the same sample region. The diffraction conditions of these DF images
132 are the same as those in Fig 3(a). Under these conditions, $BaSi_2$ grains satisfying Bragg's
133 condition of diffraction, indicated by the blue-, red-, or green-colored domain, are supposed to
134 be bright in these images; in other words, one of the three $BaSi_2$ epitaxial variants becomes
135 bright in each figure. It should be noted that the superposition of bright regions in Figs.
136 4(a)-4(c) covers the whole surface of $BaSi_2$. In Figs. 4(a)-4(c), it can be seen that the GBs are
137 parallel to the dashed lines in the blue-, red-, and green-colored $BaSi_2$ variants, respectively.
138 On the basis of this discussion, we conclude that the GBs are formed mostly from $BaSi_2$
139 {011} planes. Further discussion is mandatory to clarify why $BaSi_2$ {011} planes are likely to
140 form GBs.

141 Figure 5(a) shows the current-voltage (*I*-*V*) characteristics of the Al/*n*-$BaSi_2$ Schottky
142 diode measured at RT. The bias voltage was applied to the front Al contact with respect to the
143 sputtered Al back contact. Rectifying properties can be clearly observed. More current flows
144 when a positive bias is applied to the Al wire with respect to the back contact. These results
145 indicate that the Al/*n*-$BaSi_2$ junction forms a Schottky diode.

146 Figures 6(a)(b) and 6(c)(d) show secondary-electron (SE) and EBIC images around
147 the Al contact, respectively, with V_{ac} = 5 kV. In the EBIC method, carriers generated within
148 the diffusion length in the *n*-type $BaSi_2$ are collected by the electric field under the Al contact
149 and sensed as a current in the external circuit. In Figs. 6(c)(d), the brighter regions show
150 higher collection of electron-beam-induced carriers in the $BaSi_2$. We cannot see defect-related
151 black lines. Figure 7 shows the EBIC line-scan data along dotted line AA' in Fig. 6(c). The
152 EBIC profile shows an exponential dependence of the distance from the Al contact. In this
153 work, the diffusion length of minority carriers was roughly estimated to be approximately 10
154 μm, assuming that the EBIC profile varies as $\exp(-x/L)$, where x is the distance from the Al
155 edge (point A) along the dotted line, and L is the diffusion length of holes for $BaSi_2$. The
156 obtained minority-carrier diffusion length is much larger than the grain size of the $BaSi_2$,
157 implying that the GBs do not work as defect centers for minority carriers in *n*-$BaSi_2$. The
158 contribution of carriers generated within the *n*-Si substrate to the measured EBIC signals can
159 be excluded, because the simulated penetration depth of the electron beam is shorter than 300
160 nm, the thickness of the $BaSi_2$ layers, when V_{ac} is 5 kV. Thus, it is reasonable to think that the
161 number of carriers generated within the Si substrate was negligibly small compared to those
162 generated in the $BaSi_2$ layers. To confirm the GBs character, an EBIC system with spatial
163 resolutions less than 0.1 μm may be necessary. We should also note here that the obtained
164 minority-carrier diffusion length is roughly 30 times larger than $1/\alpha$ (=0.3 μm) at 1.5 eV,

165 suggesting that this value is large enough for solar cell applications.

166

167 **4. Conclusions**

168 We investigated the crystalline quality and GBs in *a*-axis-oriented $BaSi_2$ epitaxial

169 films grown on Si(111) substrates by MBE using RHEED, XRD, and TEM. The grain size in

170 the $BaSi_2$ films was found to be approximately 0.1-0.3 μm. Detailed investigation of BF and

171 DF TEM images and SAED patterns showed that the GBs in the $BaSi_2$ epitaxial layers consist

172 mostly of $BaSi_2$ {011} planes. The EBIC techniques revealed that the diffusion length of

173 minority carriers was estimated to be approximately 10 μm, much larger than the grain size of

174 the $BaSi_2$.

175

176 **Acknowledgements**

177 This work was financially supported by the Japan Science and Technology Agency

178 (JST/CREST). TEM observations were conducted at the Electron Microscope Facility,

179 supported in the IBEC Innovation Platform, AIST, Japan.

180

181 **References**

182 [1] C. H. Henry, J. Appl. Phys. 51 (1980) 4494.

183 [2] K. Morita, Y. Inomata, T. Suemasu, Thin Solid Films 508 (2006) 363.

184 [3] D. B. Migas, V. L. Shaposhnikov, V. E. Borisenko, Phys. Status Solid B 244 (2007)

185 2611.

186 [4] K. Toh, T. Saito, T. Suemasu, Jpn. J. Appl. Phys. 50 (2011) 068001.

187 [5] Y. Matsumoto, D. Tsukada, R. Sasaki, M. Takeishi, T. Suemasu, Appl. Phys. Express 2

188 (2009) 021101.

189 [6] D. Tsukada, Y. Matsumoto, R. Sasaki, M. Takeishi, T. Saito, N. Usami, T. Suemasu, Appl.

190 Phys. Express 2 (2009) 051601.

191 [7] T. Saito, Y. Matsumoto, M. Suzuno, M. Takeishi, R. Sasaki, T. Suemasu, N. Usami, Appl.

192 Phys. Express 3 (2010) 021301.

193 [8] M. Imai, T. Hirano, Phys. Rev. B 58 (1998) 11922.

194 [9] J. Evers, J. Less Common Met. 69 (1980) 399.

195 [10] M. Imai, T. Hirano, J. Alloys Compd. 224 (1995) 111.

196 [11] R. A. Mckee, F. J. Walker, Appl. Phys. Lett. 63 (1993) 2818.

197 [12] K. Toh, K. O. Hara, N. Usami, N. Saito, N. Yoshizawa, K. Toko, T. Suemasu, J. Cryst.

198 Growth **345** (2012) 16.

199 [13] Y. Inomata, T. Nakamura, T. Suemasu, F. Hasegawa, Jpn. J. Appl. Phys. 43 (2004) 4155.

200 [14] Y. Inomata, T. Nakamura, T. Suemasu, F. Hasegawa, Jpn. J. Appl. Phys. 43 (2004) L478.

201 [15] I. Gordon, L. Carnel, D. Van Gestel, G. Beaucarne, J. Poortmans, Thin Solid Films 516

202 (2008) 6984.

203 [16] J. Chen, T. Sekiguchi, D. Yang, F. Yin, K. Kido, S. Tsurekawa, J. Appl. Phys. 96 (2004)

204 5490.

205 [17] S. Oonishi, M. Kawamura, N. Takano, D. Hashimoto, A. Yamada, M. Konagai, Thin

206 Solid Films 519 (2011) 7347.

207 [18] H. J. Leamy, J. Appl. Phys. 53 (1982) R51.

208 [19] M. Takauji, N. Seki, T. Suemasu, F. Hasegawa, M. Ichida, J. Appl. Phys. 96 (2004) 2561.

209 [20] N. Hiroi, T. Suemasu, K. Takakura, N. Seki, F. Hasegawa, Jpn. J. Appl. Phys. 40 (2001)

210 L1008.

211

Fig.1 (a) RHEED patterns of MBE-grown $BaSi_2$ observed along the Si[1-10] azimuth (b) θ-2θ XRD pattern.

Fig.2 (a) Plan-view BF TEM image near the [100] zone axis of $BaSi_2$, and (b) SAED pattern (crystallographic orientation) obtained from the area including several $BaSi_2$ grains in the exact [100] zone axis.

Fig. 3 (a) SAED patterns obtained from single grain regions under two-beam diffraction conditions. The diffraction vectors **g** were set to three different <004> directions. (b) Enlarged SAED pattern.

Fig.4(a)-(c) DF TEM images under two-beam diffraction conditions. The diffraction vector **g** was set to be <004> for each epitaxial variant. The schematics of three epitaxial variants of $BaSi_2$ are shown. The colored domains look bright in each DF TEM image. The dashed lines correspond to {011} planes.

Fig. 5 *I-V* characteristics of the Al/n-$BaSi_2$ Schottky diode at RT.

Fig. 6 (a)(b) SE and (b)(d) EBIC images around the Al contact.

232 Fig. 7 Experimental and simulated (solid line) EBIC line-scan profiles along the dotted line

233 from points A to A’ in Fig. 6(c).

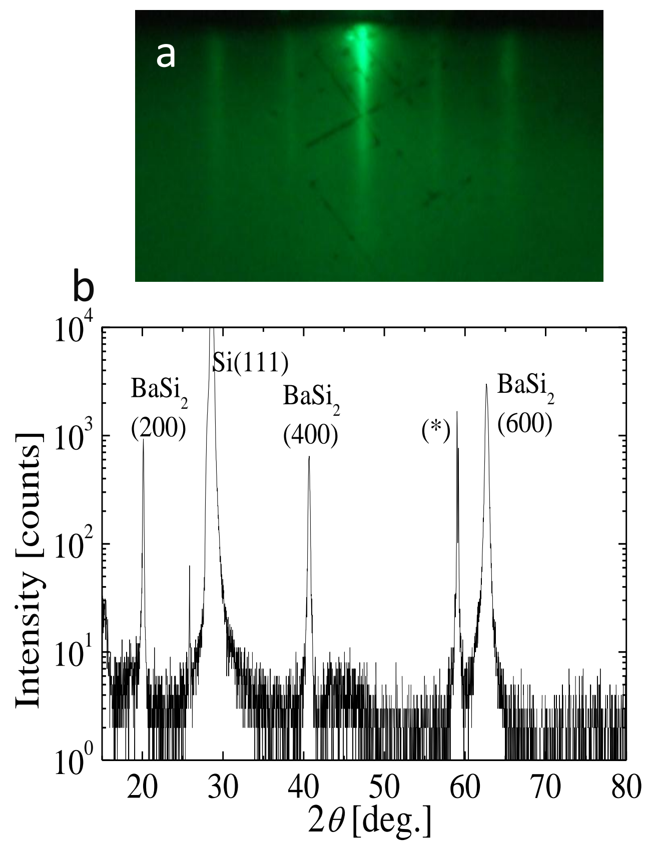

Fig. 1

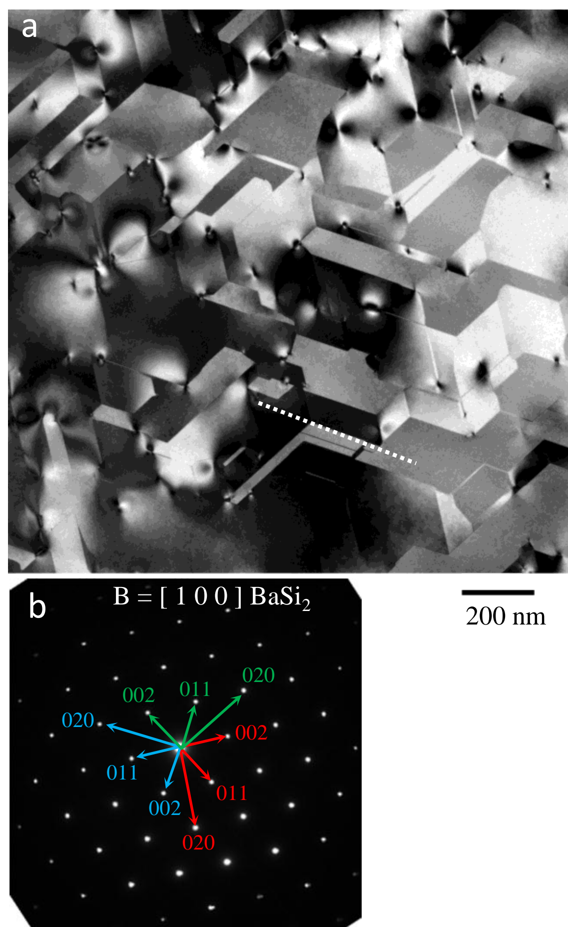

Fig. 2

a

B = [1 0 0] $BaSi_2$

(004)

g

O

(00-4)

b

(00-3)

(00-1)

(004)

Fig. 3

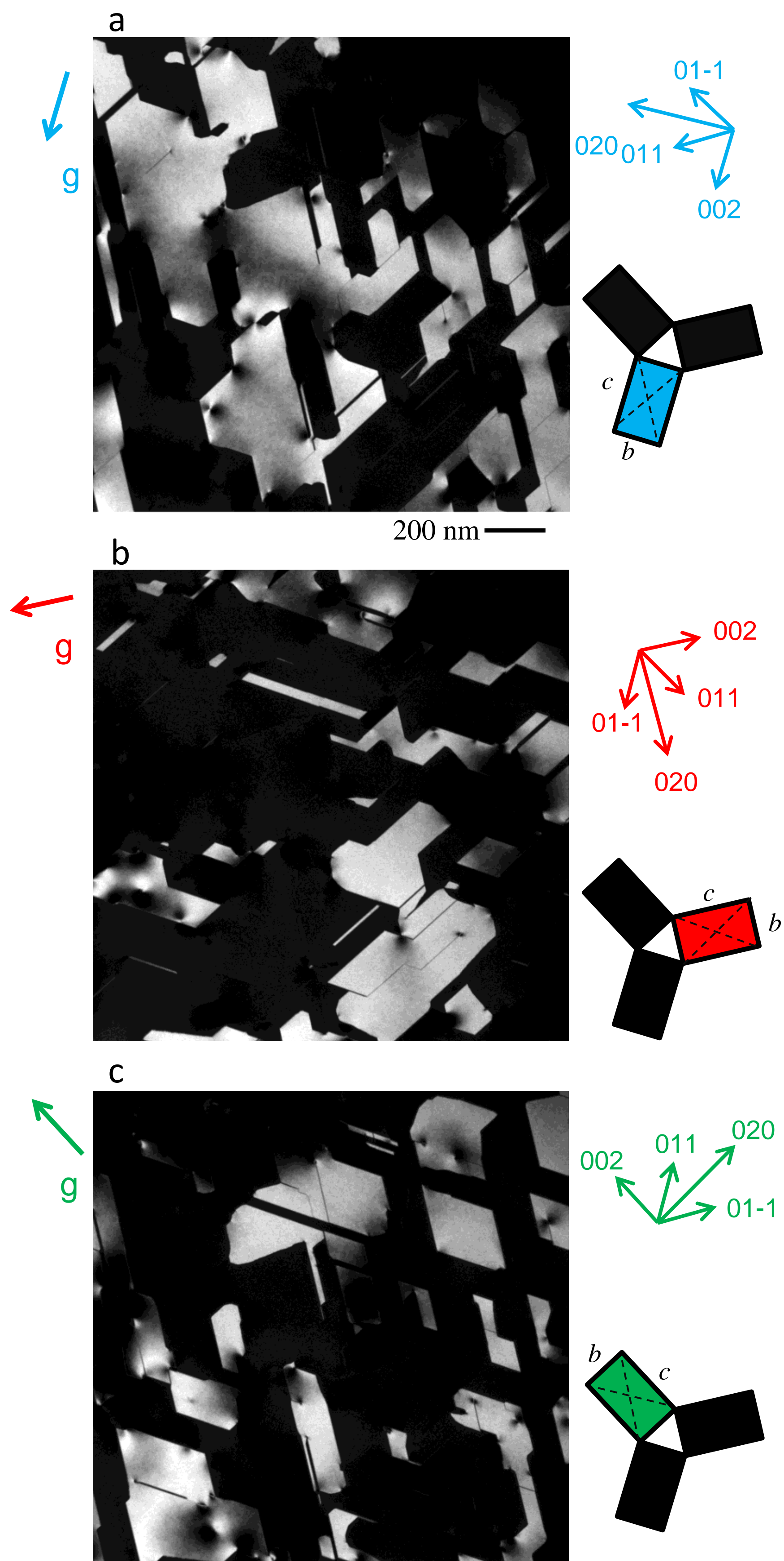

Fig. 4

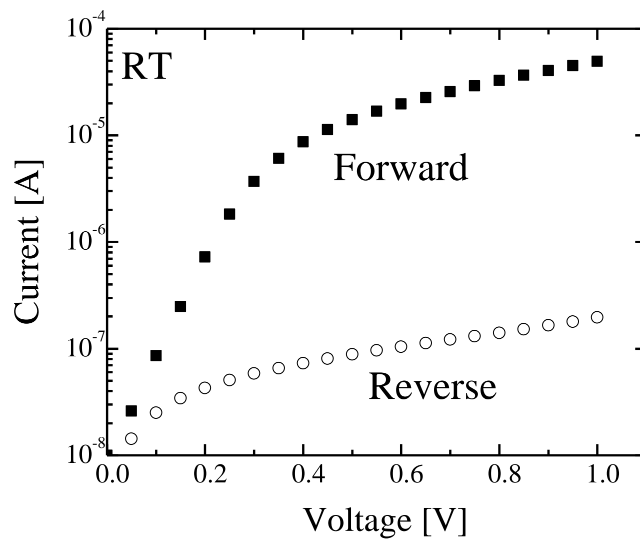

Fig. 5

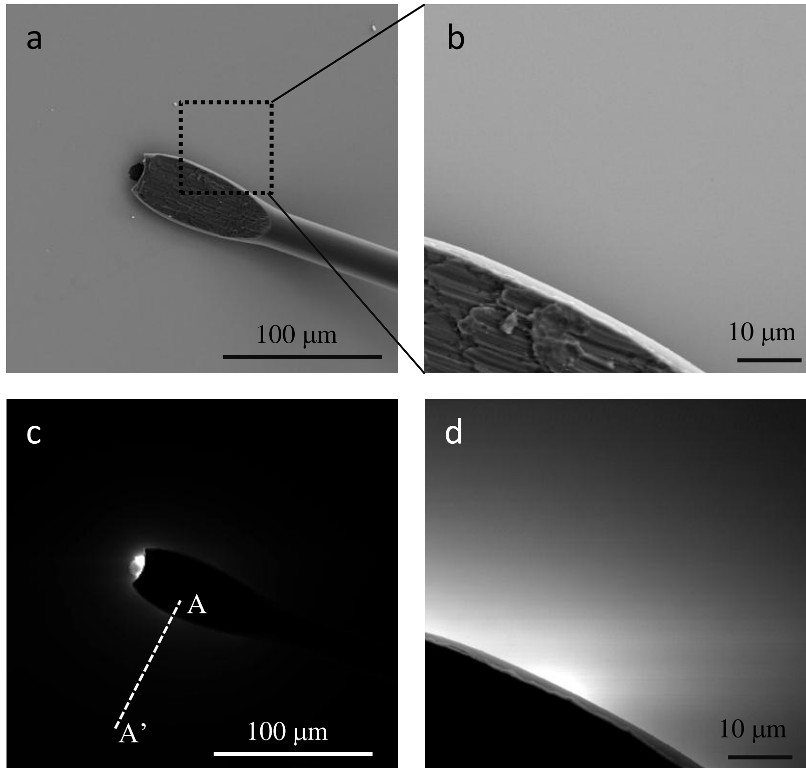

Fig. 6

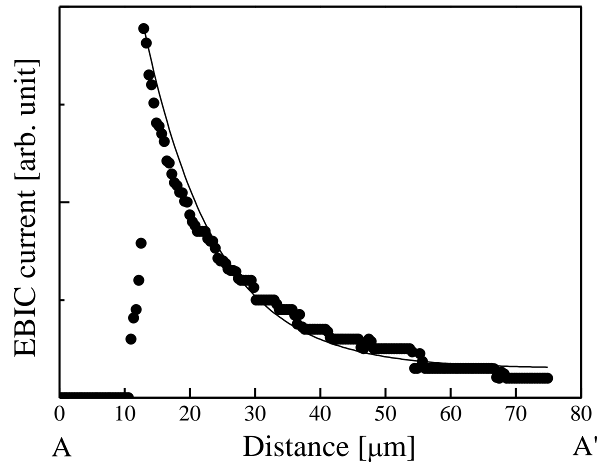

Fig. 7